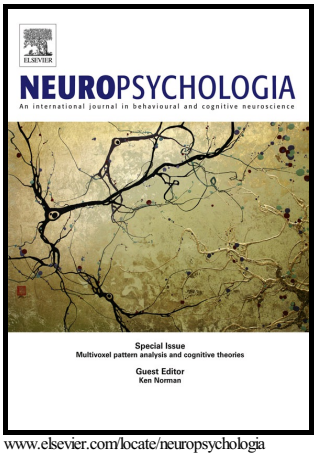

www.elsevier.com/locate/neuropsychologia

Schizophrenia: The Micro-Movements Perspective

Jillian Nguyen, Ushma Majmudar, V. Papathomas Thomas, Steven M. Silverstein, Elizabeth B. Torres

PII: S0028-3932(16)00027-0
DOI: http://dx.doi.org/10.1016/j.neuropsychologia.2016.03.003
Reference: NSY5913

To appear in: *Neuropsychologia*

Cite this article as: Jillian Nguyen, Ushma Majmudar, V. Papathomas Thomas, Steven M. Silverstein and Elizabeth B. Torres, Schizophrenia: The Micro Movements Perspective, *Neuropsychologia* http://dx.doi.org/10.1016/j.neuropsychologia.2016.03.003

Title: Schizophrenia: The Micro-Movements Perspective

Nguyen, Jillian[1], Majmudar, Ushma[2], Papathomas Thomas V. [1, 2, 3], Silverstein, Steven M.[1, 4], Torres, Elizabeth B. [1, 3, 5, 6]

[1]Graduate Program in Neuroscience, Rutgers University, Piscataway, NJ, USA
[2]Department of Biomedical Engineering, Rutgers University, Piscataway, NJ, USA
[3]Center for Cognitive Science, Rutgers University, Piscataway, NJ, USA
[4]Division of Schizophrenia Research, University Behavioral HealthCare, Rutgers University, Piscataway, NJ, USA
[5]Department of Psychology, Rutgers University, Piscataway, NJ, USA
[6]Department of Computer Science, Rutgers University, Piscataway, NJ USA

Correspondence: Elizabeth B. Torres, Sensory-Motor Integration Laboratory, Department of Psychology, Rutgers University, 152 Frelinghuysen Road, Room 116, Piscataway, NJ 08854, USA, ebtorres@rci.rutgers.edu

Abstract
Traditionally conceived of and studied as a disorder of cognitive and emotional functioning, schizophrenia (SZ) is also characterized by alterations in bodily sensations. These have included subjective reports based on self-evaluations and/or clinical observations describing motor, as well as sensory-based corporeal anomalies. There has been, however, a paucity of objective methods to capture and characterize bodily issues in SZ. Here we present a new research method and statistical platform that enables precise evaluation of peripheral activity and its putative contributions to the cognitive control of visuomotor actions. Specifically, we introduce new methods that facilitate the individualized characterization of the function of sensory-motor systems so as to detect if subjects perform outside of normal limits. In this paper, we report data from a cohort of patients with a clinical diagnosis of SZ. First, we characterize neurotypical subjects performing a visually guided pointing task that requires visuomotor transformations, multi-joint coordination, and the proper balance between different degrees of intent, among other factors. Then we measure SZ patients against the normative statistical ranges empirically determined. To this end, we examine the stochastic signatures of minute fluctuations in motor performance (micro-movements) of various velocity- and geometric-transformation-dependent trajectory parameters from the hand motions. These include the motions en-route to the target as well as spontaneous (without instructions) hand-retractions to rest. The comparisons reveal fundamental differences between SZ patients and controls. Specifically, velocity-dependent signatures show that SZ patients move significantly slower than controls with more noise and randomness in their moment-by-moment hand micro-motions. Furthermore, the normative geometric-dependent signatures of deliberateness are absent from the goal-directed reaches in SZ, but present within normative ranges in their spontaneous hand retractions to rest. Given that the continuous flow of micro-motions contributes to internally sensed feedback from self-produced movements, it is highly probable that sensory-motor integration with externally perceived inputs is impaired. Such impairments in this SZ cohort seem to specifically alter the balance between deliberate and spontaneous control of actions. We interpret these results as potential indexes of avolition and lack of agency and action ownership. We frame our results in the broad context of Precision Psychiatry initiatives and discuss possible implications on the putative contributions of the peripheral nervous system to the internal models for the cognitive control of self-produced actions in the individual with a clinical diagnosis of SZ.

Keywords

Precision medicine, micro-movements, schizophrenia, geometric transformations, visuomotor behavior, RDoC

Highlights

- The SZ patients are bradykinetic with high noise in their moment to moment micro-movements
- SZ stochastic signatures of deliberate and goal-less micro-movements are indistinguishable
- Visuomotor geometric transformations have complementary signatures in controls & SZ patients

1 Introduction

Schizophrenia (SZ) is a psychiatric disorder that is traditionally defined by impairments in high-level cognitive functions such as memory, executive function, and attention (*1, 2*). In addition to the positive, negative, and disorganized symptoms of SZ, patients also exhibit a number of motor abnormalities (*3-5*). In this sense, extensive work has documented anomalies in eye movement (*6, 7*) but abnormalities in corporeal sensations and motions have been less explored and often subjectively reported. That is, these abnormalities are perceived as exclusively observable motor output issues, leaving out reafferent sensory phenomena associated to theoretical frameworks involving internal models for the cognitive control of actions (*8-10*). The current study calls for the characterization of sensory-motor dysfunction in individuals with SZ using objective movement analytics applied to recordings of continuous movements during natural behaviors.

Recent technological advances allow for the precise quantification of subtle motor output variations that are invisible to the naked eye. However, existing analytical techniques fail to capture those subtle changes that occur from moment to moment largely beneath awareness. Part of the problem lies in the scarcity of proper statistical techniques to personalize behavioral analyses beyond homogeneous, population-based approaches. In this sense, a critical need has emerged to characterize the individual's sensory-motor signatures and their shifts during natural behaviors, particularly for pathologies of the nervous system.

Natural behaviors are a blend of deliberate and spontaneous segments with minute fluctuations in a signal's amplitude and timing (coined *micro-movements* (*11*)) that occur at imperceptible frequency- and time-scales. The continuous flow of micro-movements can also be conceived as a putative form of sensory feedback (kinesthetic reafference) (*11-14*) amplified by the muscles (*15*). Their signal and noise mixture is carried to the brain from the periphery by sensory and motor channels innervating the muscles (*16*) (**Fig 1A,B**). The associated sensory-motor noise is thought to be tied to synaptic noise (*17-19*). In goal-directed actions, motor noise unfolds and changes in quantifiable ways as the body continuously moves (*20*). Yet, the wealth of information contained in such signals is often lost when ambiguous or uninstructed goal-less movement segments are discarded as a nuisance, and/or when fluctuations in the kinematics data are de-trended and smoothed out by averaging it over a handful of trials under general theoretical assumptions of normality.

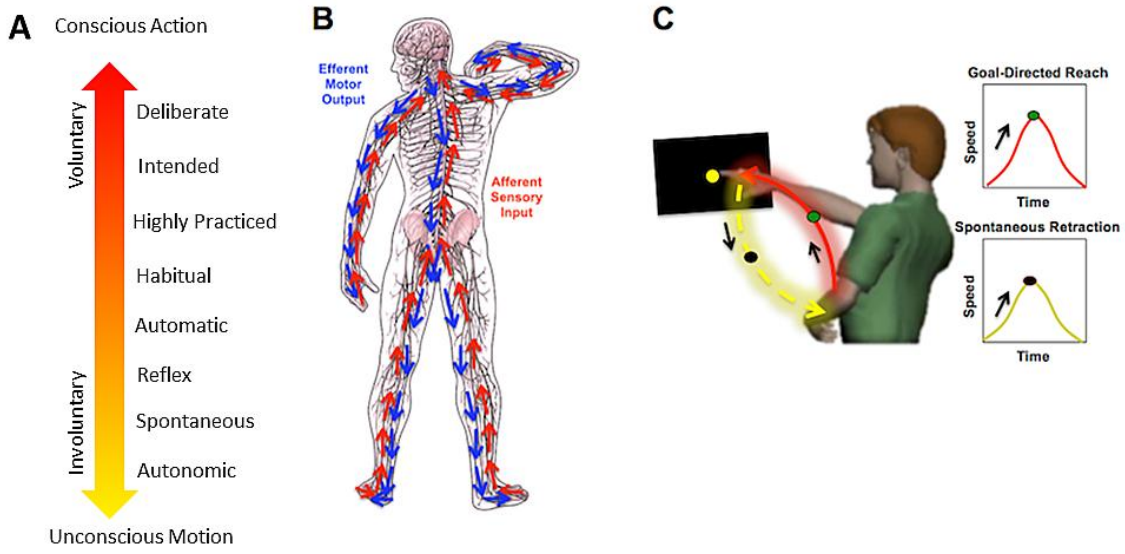

Fig. 1: New proposed paradigm to study human motions variability and its impact on motor reafference.
Movement can be defined over a continuum (A), spanning conscious, voluntary actions, to involuntary functions of the autonomic nervous system. Each level of functionality contributes to the shaping of the statistical features of complex human behaviors, yet most research focuses solely on the deliberate component of this spectrum without attending to the balance across these complementary and interrelated modes. (B) Schematics of the flow of afferent and efferent signals to and from the central nervous system and the periphery. Movement variability as a form of kinesthetic re-afference can inform of the balance between movement classes, serving as a physical, quantifiable readout of fluctuations in sensory-motor noise-to-signal ratios. (C) Experimental task employed in this study to characterize motions that are goal-directed (red) and uninstructed goal-less (yellow) to better understand the continuous flow of movement along different levels of intent.

==========

Recent works highlight the importance of characterizing patterns of kinesthetic reafference through micro-movement analyses in neurological conditions such as autism spectrum disorders (ASD) (*11*), Parkinson's disease (*21*), as well as during coma states after brain injury (*22*). This work has uncovered objective dynamic biomarkers that blindly identify sublevels of severity in these different pathologies of the nervous system; these data have also distinguished spontaneous random fluctuations in performance from well-structured systematic fluctuations. The methods have served to track the effectiveness/risk of psychotropic drug use, and have been utilized in clinical trials (*23*). Therefore, it is potentially useful to apply these methods to the study of SZ, a disorder that, in addition to perceptual and cognitive/emotional deficits, also involves problems with corporeal awareness (*24*). It will be important to understand issues with corporeal awareness in SZ and to elucidate the overall impact that sensory-motor abnormalities may have on cognitive and emotional impairments. The characterization of patterns of micro-motor output variability may lead to the discovery of unknown pathophysiology underlying this devastating brain disorder.

Reports of motor disturbances in populations exhibiting core symptoms of SZ by today's diagnostic criteria date as far back as the late 1800's. For example, catatonia, previously classified

as a subtype of SZ in the DSM-IV, was first defined motorically: abnormal body posturing, muscle rigidity, spasms, jerking, and decreased responsiveness were observed in patients (*25, 26*). However, theories treating the psyche as a separate entity from the body led to a shift in focus towards cognitive impairments and away from sensory-motor dysfunction (*27, 28*). Influenced by this trend, researchers focused their efforts on understanding high-level cognitive processes, almost to the exclusion of exploring the body's role in embodying these mental states, widening the gap in knowledge on mind-body relationships. These symptom-based approaches have severely impeded the biological characterization of mental disorders from a physiologically-relevant viewpoint (*29, 30*). Fortunately, in recent years, theories of embodied cognition have gained traction, reestablishing the importance of linking mind and the body to recognize the contributions of sensory-motor processes on scaffolding and shaping high-level executive functions (*31-33*).

A large body of evidence suggests that individuals with SZ exhibit problems in sensory-motor integration, persistence of primitive reflexes, and problems in the execution of complex motor acts (*3, 34*). However, little is known in SZ about sensory-motor integration processes and visuomotor coordinate transformations at various levels of perceptual awareness. Here we introduce a newly defined class of uninstructed supplementary movements that, to our knowledge, has not been well studied within the SZ population. As the current focus remains on assessing levels of volitional control (and sometimes the lack thereof) (*35-38*), we study such transitional motions in the context of goal-directed behavior. The types of covert, goal-less motions that spontaneously occur without instructions are not commonly studied in general (*39*). Yet, they can be revealing of specific sources of sensory guidance to aid overcome visuomotor deficits (*40, 41*). These segments of natural behaviors aid in the fluidity of movements and support goal-directed segments. They also help in predicting the sensory consequences of future actions in different contextual situations (*42*) (**Fig 1A**). The new methods presented here analyze the continuous stream of motions including micro-movements blended in goal-directed and goal-less motions. We aim at shedding light on the possible roles of sensory-motor noise in the types of geometric transformations that inevitably take place during visuomotor tasks.

The present work is in line with the new concept of *Precision Medicine* (*43*). Precision medicine is a new approach to acquire and integrate knowledge from biomedical research and clinical practices. It is a computation-enabled platform poised to radically transform the ways in which we currently conduct biomedical research and patient care. Within this new platform, the statistical framework introduced here speaks specifically of the new initiative by the National Institutes of Mental Health (NIMH) regarding Precision Medicine for Psychiatry. More explicitly, we refer to the Research Domain Criteria (RDoC) initiative (*44*). Although a module for sensory-motor issues does not yet exist in the current RDoC design, present evidence is in favor of this consensus (*45*). Here we present the application of our micro-movements paradigm (**Fig. 2A**) and statistical platform for individualized behavioral analyses to objectively characterize patterns of sensory-motor noise in SZ during a simple pointing task (**Fig. 2B,C**).

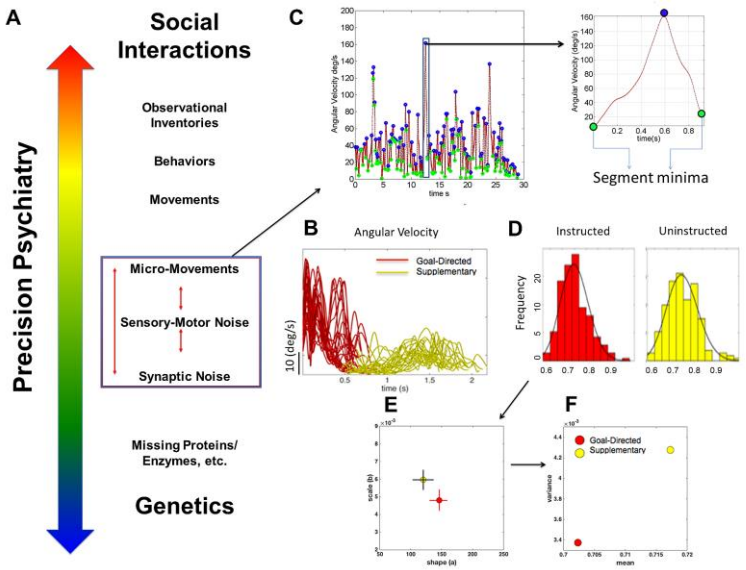

Fig. 2: The Contributions of Micro-Movements to Sensory-Motor Behavior
(**A**) The spectrum of precision psychiatry in which SZ can be characterized at various levels, spanning from socio-motor behavior to genetics is illustrated in schematic form. Visible movements, which make up our social behaviors, contain as well imperceptible minute fluctuations (micro-movements) that can be physically quantified non-invasively using recent advances in technology. This allows for the study of signatures of sensory-motor noise arising from transduction and transmission of sensory signals from underlying sensory and motor nerves. This layer of analyses highlighted inside the box is the focus of the proposed research program. The signatures of sensory motor noise can then be mapped to specific forms of synaptic noise directly tied to genetic factors. In this way efferent and afferent (exo-and endo-afferent) contributions to the underlying pathophysiology of SZ can be characterized for idiopathic cases in relation to cases of known etiology. (**B**) Micro-movement statistical signatures are estimated using speed-dependent parameters in both goal-directed (red) and supplementary (goal-less) movements (yellow). Movements are separated into each class according to level of instruction (see text). The data are mean centered and the maximal fluctuations (peak angular velocity) are gathered and normalized (see text and illustration inset in (**C**)). Frequency histograms are obtained with optimal binning. Using maximum likelihood estimation, the underlying probability distribution that most likely fits the histograms of the fluctuations is obtained separately for each movement class. (**D**) The estimated parameters from the continuous Gamma family of probability distributions, the shape (***a***) and scale (***b***) are plotted on the Gamma plane with 95% confidence intervals (**E**). Points on this map represent the individuals' signatures and provide a characterization of the stochastic signatures of the moment-by-moment speed-dependent fluctuations. (**F**) The estimated Gamma mean and variance are also plotted on the Gamma statistics plane for the given trajectories using the empirically estimated shape (***a***) and scale (***b***) parameters.

2 Materials and Methods

2.1 Participants

Written informed consent was obtained from all participants. The study was approved by the Rutgers University Institutional Review Board. Compensation was provided to participants.

Our subject sample consisted of 24 neurotypical controls (20 males, 4 female) and 23 schizophrenia patients (18 males, 5 females) (**Table 1**).

	Patients		**Controls**	
Parameter	**Mean**	**S.D.**	**Mean**	**S.D.**
Age	42.83	11.99	44.04	12.68
Years of Education (Self)	12.26	2.32	13.41	1.56
Years of Education (Father)	10.82	3.85	11.35	3.32
Years of Education (Mother)	11.18	3.89	10.75	3.53
Ethnicity (% Caucasian)	39.13%	N/A	54.17%	N/A
Gender (% Male)	78.26%	N/A	79.17%	N/A
Handedness (% Right Handed)	78.26%	N/A	87.5%	N/A

Table 1 Demographic Information for Patients and Controls

First (mean) and second (variance) moments from the normal distribution obtained from the demographic data of patients and controls. Patients ranged from ages 22-57 (median age 47), whereas controls ranged from ages 18-64 (median age 45). Controls were recruited to match subjects as closely as possible to patients based on these listed demographic parameters.

For all subjects, the inclusion/exclusion criteria included the following:

- Normal stereoscopic vision
- Normal or corrected-to-normal visual acuity
- Age 18–65 years
- No clinically significant history of head injury or loss of consciousness
- No diagnosis of neurological disease
- No diagnosis of mental retardation or pervasive developmental disorder
- No substance dependence in the past six months

Additional criteria for the control group included:

- No Diagnostic and Statistical Manual of Mental Disorders, Fourth Edition, text revision (DSM–IV–TR) diagnosis of schizophrenia or any other psychotic or mood disorder
- No current psychotropic or cognition enhancing medication

Additional criteria for patient population:

- DSM–IV diagnosis of schizophrenia (SZ) or diagnosis of schizoaffective disorder (SA)

Patients were recruited from the Rutgers University Behavioral Health Care clinics. Patients were either enrolled in the extended partial hospital program (PHP) or were outpatients that only required biweekly or monthly visits to healthcare providers. The extended PHP provides patients that are still going through the stabilization process (from the stabilization to the stable phase) with continual structured daily support before they are ready to move on to outpatient status. There were 13 patients enrolled in the extended PHP and 10 patients were in the outpatient program. Of the 23 patients, 18 participants had a diagnosis of SZ, while the remaining 5 were diagnosed as SA.

2.2 Motion Capture

We used 13 electromagnetic sensors at a sampling frequency of 240 Hz (Polhemus, Liberty, Colchester, VT) and motion-tracking software (The Motion Monitor, Innovative Sports Training, Inc., Chicago, IL) for continuous motion capture. Sensors 1-12 were placed on the following body segments using modified sports bands and athletic gear designed to optimize unrestricted movement of the body: center of the forehead, the trunk at thoracic vertebrate T12, right and left scapula, left upper arm, left forearm, left wrist, right upper arm, right forearm, right wrist, right hand index finger, and right hand thumb. An additional sensor was used to digitize the body to construct a biomechanical model using the Motion Monitor software. The remaining sensor was placed on the backside of the display screen behind the approximate location of where the target appears during the experiment. We recorded the full motor response of each participant in real time both in the forward motion (from initiation of hand movement up to the touch of the target), and in the non-instructed, automatic retraction of the arm back to the table during the pointing task.

2.3 Stimulus Apparatus and Experimental Procedure

Once all sensors were donned and calibrated, subjects were seated at a table facing a touchscreen display. An in-house developed MATLAB (Release 2014b, The MathWorks, Inc., Natick, Massachusetts, United States) program controlled the presentation of targets on an iPad touch display (Apple, Cupertino, CA) and recorded the touches. The MATLAB program was presented on the iPad using the AirDisplay iOS application (Avatron Software). Each target consisted of a filled yellow circle on a black background (**Fig. 1C**). The circle was located in the middle of the display screen. Participants were instructed to touch the target with their dominant hand starting from the edge of the table, but were not given any instructions about the retracting motions back to rest. Upon touching the target, the yellow circle disappeared briefly (for 300ms) and then reappeared. The location of the target remained the same across trials. Participants were told to continuously reach for targets once the experimenter instructed them to begin. Each segment of continuous data acquisition lasted 15 seconds, and then the data was saved upon a beep indicating to the participant stop briefly. The auditory cue marked the end of each 15s continuously recording interval. Participants repeated the same procedure for each trial until at least 100 successful touches were recorded via the MATLAB program.

2.4 Data Analysis

Definition of micro-movements: Small trial-by-trial variations in performance as captured by fluctuations in the amplitude or the timing of critical kinematic parameters. These may include velocity- and acceleration-dependent parameters such as the maxima, the minima, and the times to reach the peaks, or the inter-peak interval timings along a continuous time series of changes in the positions of some parameter, etc. This definition should not be confused with small movements or with sub-movements comprising a single movement or motor sequences. The present paper assesses the trial-by-trial velocity-dependent variations, as well as variations in a geometric symmetry from the hand trajectories. The analyses refer to the stochastic signatures of those minute motor variations, their accumulation, and individualized empirically estimated statistical features.

Motor hand trajectories were decomposed into movement classes with different levels of instruction. In each trial, the explicitly instructed goal-directed reach (forward motion to the target) was separated from the uninstructed goal-less retraction of the hand (backward motion to rest).

We call these supplementary segments. The latter was freely chosen by the participant without any instructions. To separate the two segments of the continuous reach loop, the forward trajectory was automatically identified using in-house developed software with MATLAB. Reliable criteria for automated parsing used the touch point, where the speed profile of the trajectory has near instantaneous zero linear velocity, the hand-to-target distance which decreases to 0-value, and the touch screen position and time which were also registered (**Fig. 1C**). We analyzed data from the sensor located on the index finger of the dominant hand for this research article. Results from analysis of the remaining 12 sensors and the sensor located at the target are beyond the scope of this paper and will be disseminated in future work.

2.5 Speed Profiles

We assessed the moment-by-moment motor output variability from the angular velocities in each movement class for each subject (**Fig. 2B**). To this end we obtained the peak angular velocity in each segment and gathered all peaks over the entire session for each segment type (forward and backward). These data were mean-centered to obtain the maximal deviations from the mean.

To avoid allometric effects (*46*) due to different anatomical sizes across different subjects, the data were normalized by dividing the peak velocity between two local segment minima by the sum of the peak velocity and the average velocity between the two minima (**Fig. 2C**). These normalized angular velocity indexes were gathered in a frequency histogram with proper binning **Fig. 2D)** (*47, 48*). Using maximum likelihood estimation we then obtained the shape *(a)* and scale *(b)* parameters of the continuous Gamma family of probability distributions with 95% confidence regions (**Fig. 2E**).

The Gamma probability distribution function is given by: $y = f(x|a,b) = \frac{1}{b^a \Gamma(a)} x^{a-1} e^{\frac{-x}{b}}$, in which a is the shape parameter, b is the scale parameter, and $\boldsymbol{\Gamma}$ is the Gamma function (*49*). We can capture individualized velocity-dependent fluctuations from trial to trial by examining the stochastic signatures estimated from each person's movements as (*shape, scale*) points on the Gamma plane (**Fig. 2E**). These stochastic signatures on the Gamma plane range from Gaussian-like symmetric distributions of average speed patterns found in typical adult systems (*39*), to exponential distributions found in compromised systems concerning pathologies such as autism, posterior parietal cortex stroke and Parkinson's disease (*11, 40, 50*). The latter values are located to the left of the horizontal (shape) axis on the Gamma plane, while the former are to the far right with skewed distributions in between the two extremes. In general, power-law distributions of velocity-dependent indexes are found across the human life span. In the present work we use the Gamma distribution analysis to characterize potential differences between the different movement types generated according the level of instructions by each individual subject in each of the control and schizophrenia groups.

The empirical estimation of the appropriate family of probability distributions to characterize sensory-motor control counters traditional approaches. The latter simply assumes normality by applying the theoretical Gaussian distribution, taking the mean and variance of kinematic parameters linked to motion trajectories averaged across a relatively small number of trials. This process tends to smooth out the velocity-dependent fluctuations that we track from trial to trial and use here in the statistical parameter estimation procedure.

In the traditional approaches where the theoretical distribution is rather assumed and its moments used without empirical proof that the assumption is valid, the statistical power is attained by examining a large number of subjects, often pre-selected to be in some homogeneous group, then the different groups are compared under the significant hypothesis testing paradigm using

some parametric model which assumes as well homogeneity of variance and linear (additive relations). In the present paradigm the statistical power of the estimation procedure lies in the number of samples used to make the robust estimate (at least a hundred per person). In this sense we use the angular velocity peaks as a parameter of interest because in point-to-point movements, such as these forward-and-back target-directed pointing motions, the linear velocity would yield two peaks, one forward and one backwards so we would need at least 100 reaches. This would tend to induce fatigue-related effects towards the end of the session. Using the angular velocity instead yields more peaks for the estimation process with fewer trials, being as well less taxing on the participant. Furthermore, the normalization of the continuous angular speed from local minima to local minima scales the waveforms across subjects despite the anatomical differences that tend to affect the distance traveled per unit time (*51*).

In summary, for practical purposes it is best to use kinematic parameters with higher frequency of peaks. In this sense, one can attain higher statistical power for the individualized estimates of the distribution parameters within less time when the waveform is the angular rather than the linear velocity. In the clinical settings (where we ultimately would like to use this approach) 15-20minutes tend to be the time period of a visit. Within this time frame it is possible to provide a robust statistical estimate in a timely fashion at the clinic if we use kinematics parameters with higher frequency of peaks (besides the linear velocity which yields fewer peaks per unit time, e.g. (*42*), (*11*) and require longer sessions.) **Figure 2C** shows an example of the raw angular speed trace and the waveform of one local peak between two local minima isolated to be scaled using the normalization procedure:

$$Npeak V = \frac{peak V}{peak V + avrg V_{local\ \min - to - local\ \min}}$$

Here we take the velocity peak between two local minima and divide it by the sum of the average velocity between those two local minima and that local peak velocity value. This is done for each local peak so as to scale the waveform of interest. The estimation of the Gamma first and second moments (mean and variance) for each subject uses the estimated Gamma shape and scale parameters (**Fig 2F**). The variance $\boldsymbol{\sigma_W^2 = a.b^2}$ and the mean $\boldsymbol{\mu_W = a.b}$, in which $\boldsymbol{W}$ refers to the movement segment window, i.e. the forward goal-directed reach or the uninstructed retraction.

We then use the estimated Gamma mean and Gamma variance to compute the noise-to-signal ratio, i.e. the Fano Factor (*52*), $\boldsymbol{FF = \frac{\sigma_W^2}{\mu_W}}$, which reduces to the Gamma scale parameter $\boldsymbol{b}$. Therefore, as the value of $\boldsymbol{b}$ increases, so does the noise-to-signal ratio. Recent work reveals that these parameters shift as sensory-motor behavior adapts to external stimuli, providing an index for the human motion parameter range for values of the Gamma shape $\boldsymbol{a}$. It has been found that pathological cases fall at or near $\boldsymbol{a}$*=1* (*11, 40, 53*), which corresponds to the special case of the memory-less exponential distribution. In marked contrast, when probability distributional analyses were performed on fluctuations in motor performance in skilled athletes, the predictive value of the speed-dependent parameters in their impending trajectories have symmetric, Gaussian-shaped distributions (*39*). Furthermore, during repeated motor performance, fatigue may also contribute to motor variability and impact the noise to signal ratio when comparing earlier to later trials of a session, as the average speed tends to decrease when the muscles fatigue (*54*). These novel findings set bounds on these parameters that will help us interpret results in the context of SZ.

In addition to estimating the shape ($\boldsymbol{a}$) and scale ($\boldsymbol{b}$) parameters, means ($\boldsymbol{\mu_W}$), and variances ($\boldsymbol{\sigma_W^2}$) for each participant, we determine the line that best fits the scatter of the log-log plot of the Gamma parameters in each movement class for each subject. Previous work reported exponential decay of the noise in the hand linear and angular velocities characterizing micro-movement variability in humans (*42*) subject to stochastic rules with multiplicative error. Importantly in typical controls such rules, when expressed in terms of the log of the parameters, provide linear relations of the trial by trial noise evolution so as to be able to predict impending speed from current linear velocity and acceleration (*39, 42*). Yet these relations are violated in autism spectrum disorders where the noise is best characterized by the 'memoryless' signature of the exponential distribution (*11, 53*). In such cases the limiting case of the Gaussian distribution with high values of the shape parameter, towards the right of the Gamma parameter plane, are not attained and the log-normal distribution also fails to characterize such speed dependent noise in ASD.

To assess the departure from the linear relation between the log of the shape and the log of the noise on the scatter plotted on the Gamma parameter plane, denoting such error as delta ($\boldsymbol{\Delta}$), we obtained the normal distance from each point (for each participant) in the scatter to the unit line of the power fit to the log-log of the empirically estimated Gamma parameters. We calculated this for each subject in each movement class. Delta is an estimate of the standard deviation of the error in predicting a future observation at each point with respect to the empirically estimated coefficients of the fitted polynomial function to the log of the parameter. The slope of this line is the exponent of the power relation that we uncovered between the shape and scale Gamma parameters describing the probability distribution of the angular trajectory parameters. The delta error gives a sense of departure of each subject data from the theoretical power law relation. In other words it tells us about the failure to predict future speed-dependent events from current ones. We then take delta values for each participant and map them against the Fano Factor. As explained above, this is a measure of dispersion for the estimated distribution. Thus we gain information about the noise levels and the speed dependent predictive power of each person, their normative ranges and possible break downs in the integrity of the sensory-motor systems of the individual with SZ.

We employ the Wilcoxon Rank Sum test to determine if velocity-dependent parameters derived from each movement class statistically differ from one another in our control and patient groups. The Wilcoxon Rank Sum Test is a nonparametric test that assesses whether or not population median ranks differ (*49*). We applied the Wilcoxon Rank Sum Test to the Fano Factor calculations and the delta values associated with each condition.

2.6 Geometric visuomotor transformation metrics: Rationale

Visuomotor transformations for reaching and grasping actions require the solution of many difficult computational problems (*55*). Two of these problems were originally posed by Nikolai Bernstein (*56*). One is known as the redundancy problem, whereby a unique reach solution must be found to systematically map the many internal degrees of freedom (DoF) of the physical body to an external goal (or set of goals) so as to consistently coordinate those DoF in an efficient manner (e.g. (*57*)). The other problem relates to the first conjecture, as despite the uniqueness of the overall solution, the system exhibits small variations around the solution when it repeatedly performs the same action. From moment-to-moment these fluctuations around the solution (which we have coined here micro-movements) provide feedback on task compliance, habituation and/or fatigue, as well as an estimate on the degree of stochastic feedback that the system may be receiving from moment-to-moment, among other factors of performance. Here we combine both the redundancy-problem and the variability-problem in the tracking of this geometric coordinate-transformation symmetry to assess: (1) the degree to which the mental intention to reach the target mismatches

the physical volitional control of the reach in SZ patients, and (2) the degree to which the moment-to-moment stochastic feedback of velocity-dependent signals impedes task performance in relation to controls. The Appendix further provides an explanation regarding the theoretical aspects of these geometric ratios.

Area-Perimeter Ratio Error Triangulation

Hand trajectories in the goal-directed reaches and automatic retractions for each subject were resampled to *4x* the number of points in each trajectory in order to generate a unit speed curve and provide a large number of equally spaced intervals along the curve. This was performed using in-house developed geometric methods that preserve the geometric path of the curve. It is important to accurately estimate (using the Riemann integration method) the area and perimeter enclosed between the curved reaching trajectory which is a non-Euclidean straight line with respect to a non-Euclidean metric and the Euclidean straight line joining its two ending points (i.e. the starting hand location and the target). Sample raw trajectories are shown in **Fig. 3A, B** for a representative control subject and **Fig. 3D, E** for a representative patient. The trajectory symmetry ratio (to be explained next) is determined for each trial using information about the maximal bending of the curved traced by the hand (marked on each trajectory of **Fig. 3A, B and D, E**). Representative scatters of these trajectory symmetry ratios are depicted in **Fig. 3C** for the representative control and in **Fig. 3F** for the representative patient. Notice that the patient breaks down the scatter relation to the line of unity for both forward and back cases and has a shifted scatter centroid away from the symmetry.

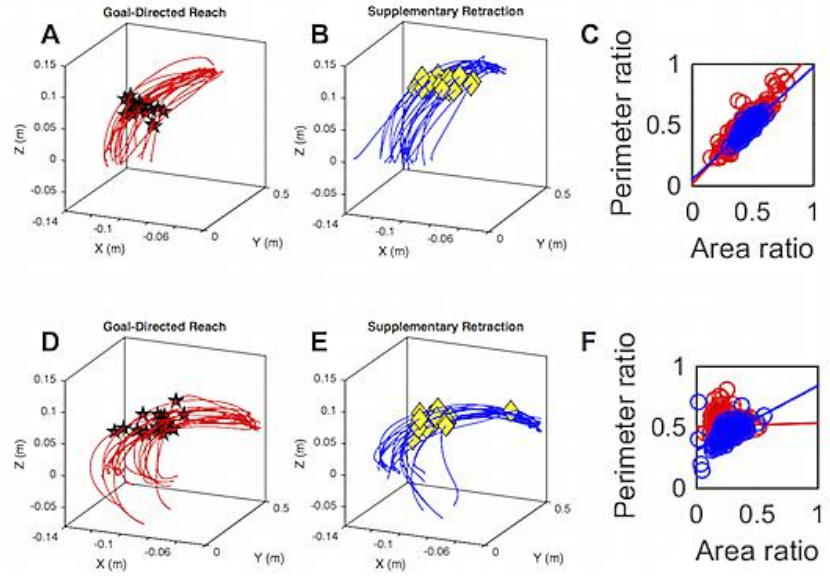

Fig. 3: Sample Trajectory Data for Controls and SZ Patients

(**A**) Forward trajectories from a representative control pointing the hand towards the target. (**B**) Backward trajectory from the same control as the hand retracts to rest. (**C**) Area-perimeter ratio values associated with each movement class (red for goal-directed and blue for goal-less). (**D-F**) Forward and backwards hand trajectories and area-perimeter ratios are plotted from a representative SZ patient. Landmarks of interest are the points of maximum bending in the hand path trajectories. These are indicated by the black stars (forward) and yellow diamonds (retractions). The colored lines in **C-F** indicate the lines of best fit to each area-perimeter ratio scatter.

==========

In **Fig. 4** we graphically explain the process of determining the ratios. **Fig. 4B** graphically illustrates the Euclidean straight line from the initial hand position to the baseline target location (filled black circle). Each point in the resampled trajectory is then projected onto each corresponding point on the straight line. The partial area (colored in yellow in **4B**) enclosed between the curve and the straight line is obtained up to the point of maximum bending (red star ($\boldsymbol{\kappa_{max}}$)), denoted $\boldsymbol{A_{partial}}$. We also obtain the total area, $\boldsymbol{A_{Total}}$ between the curve and the line and their partial to total ratio is calculated. When the coordinate transformation is distance metric preserving (an isometry), this ratio is **½** (*58*) as explained above.

The perimeter ratio was determined in a similar fashion, dividing the partial perimeter ($\boldsymbol{P_{partial}}$) by the total perimeter. The partial perimeter is the sum of the path length of the curve traced by the hand in route to the target, starting from the initial hand position to $\boldsymbol{\kappa_{max}}$ and the corresponding straight line segment, including the normal distance segment from the curve to the line at $\boldsymbol{\kappa_{max}}$. The total perimeter, $\boldsymbol{P_{total}}$ is given by the sum of the curve and line lengths along the entire hand path and the straight line, ($\boldsymbol{P_{ratio} = P_{partial}/P_{total}}$) (**Fig. 4B**).

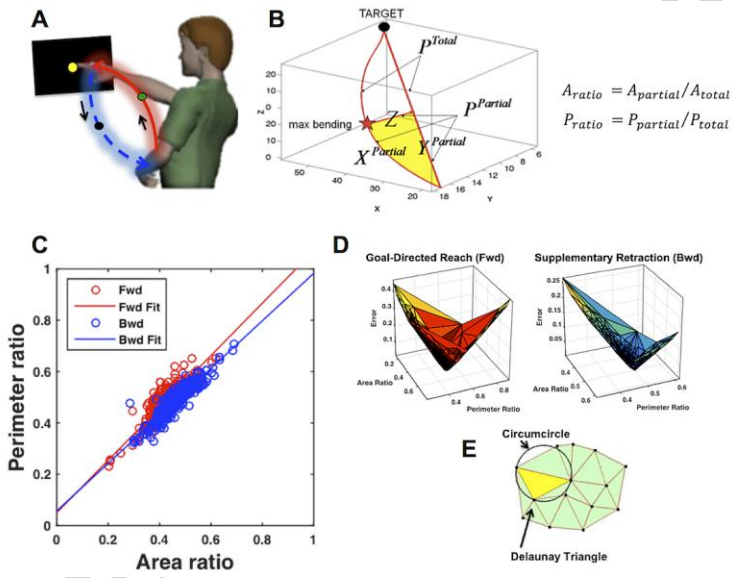

Fig. 4: Area-Perimeter Ratio Analysis
Graphical representation of the geometric analyses of hand trajectories, involving the following steps: **(A)** Gather the forward and backward hand trajectories. **(B)** Project the curved hand trajectory on the Euclidean straight line joining the initial position of the hand and the final target location. Obtain the point of maximal bending where the curve is at maximal normal distance from the line (red star). Compute the partial area enclosed between the line and the curve up to that point (shadowed in yellow) and divide it by the total area. This ratio is normally ½ and typically resembles the perimeter ratio, which is obtained in a similar fashion using the partial and total perimeters (see text for details). **(C)** Plot the area ratio and the perimeter ratio for each trajectory along with a linear fit. The error from the linear fit is obtained as a third dimension and a surface fit to the scatter using Delaunay triangulation **(D-E)** for each of the goal-directed (forward) and goal-less (retraction) segments.

==========

We use this coordinate-transformation theoretical relation to characterize avolition in SZ patients. To this end we introduce the notion that if both movements (forward and back) follow the symmetry there is good balance between the volitional control of the deliberate phase of the pointing motion but more importantly there will be good volitional control of the spontaneous (uninstructed retraction) even when this motion went reportedly unnoticed by the person. The break down in the relation between the two motions and the lack of symmetry compounded with high noise in the scatter are all indicative of a break down in the theoretical geometric relations. But also, given our previous empirical evidence in patients where coordinate transformations break down due to stroke in the Posterior Parietal cortex, or due to noisy kinesthetic reafference in PD, we here can investigate in SZ patients the extent to which these issues with sensory-motor integration are present.

We first estimated the normative ranges of the Gamma parameters with respect to the hand trajectory ratios and then estimated the SZ ranges in relation to the normative data. In **Fig. 4C** we illustrate sample area-perimeter ratios for forward reaches in red and uninstructed retractions in blue. Ideally, the geometric transformation of the area-perimeter ratio should fall on a straight line with a slope of 1, signifying that the balance between both spatial parameters is equal ($\boldsymbol{P_{ratio}} = \boldsymbol{A_{ratio}}$). We calculate the error of each area-perimeter ratio value by determining the shortest normal distance to the line $\boldsymbol{y} = \boldsymbol{mx}$, in which $\boldsymbol{y}$ is the $\boldsymbol{P_{ratio}}$, $\boldsymbol{x}$ is the $\boldsymbol{A_{ratio}}$, and $\boldsymbol{m} = \boldsymbol{1}$. Since we now introduce a third dimension to our data, the error $\boldsymbol{E}$, we can generate a 3D surface representation of all three variables to perform topological and geometric queries (**Fig. 4D, E**). To this end we built a matrix with values for all $\boldsymbol{A_{ratio}}$, $\boldsymbol{P_{ratio}}$, and $\boldsymbol{E}$ for each subject and movement class, and created a surface on the three-dimensional scatter.

Delaunay triangulation creates a surface representation of a matrix $\boldsymbol{P}$ out of triangles connected by points $[\boldsymbol{x}, \boldsymbol{y}, \boldsymbol{z}]$ in each row of matrix $\boldsymbol{P}$, each point serving as a vertex, such that the circumcircle associated with each triangle thus formed contains no other points in matrix $\boldsymbol{P}$ in its interior (*59*). **Fig. 4E** demonstrates an example of how Delaunay triangles are constructed in 2D, and **Fig. 4D** illustrates the surfaces formed from the sample data found in **Fig. 4C**, in which the two panels of **Fig. 4D** represent the surface generated by forward goal-directed reaches (left) and the surface generated by the spontaneous retractions of the hand (right).

We then calculated the areas of the triangles (**Fig. 4D**) that make up each 3D surface, and found the parameters that most likely determined the underlying probability distribution for each movement class. We applied the statistical framework presented for the speed-dependent parameters on these new kinematic spatial metrics to understand how they unfold in the forward goal-directed reach and the spontaneous, uninstructed retraction. The Gamma parameters were estimated based on the Gamma probability density function fitted to each participant's probability distribution of triangle areas. We then took the log of the shape ($\boldsymbol{a}$) and scale ($\boldsymbol{b}$) parameters and found the first-degree polynomial function that best fits the grouped data in a least-squares sense. We calculated delta (the error of the point in the scatter to the line, as measured by the orthogonal distance from the point to the line) for each group and mapped delta values against the Fano Factor calculations. For visualization purposes these are presented as scatter-box plots.

3 Results

3.1 Assessment of Executive Dysfunction in Patients with SZ

The average Frontal Systems Behavior Scale (FrSBE) Score for executive dysfunction was 59.5 +/- 17.14 for the entire clinical population (**Table 2**). Scores between 65 and 130 are considered to

be within the clinical range, whereas any scores between 60 and 64 are considered borderline. Note that we see high variance in scores, as approximately half of the patient group (n=11) scored as exhibiting executive dysfunction, while others did not. We therefore find evidence for heterogeneity in the population under study. It should be noted that, if we included individuals in an acute psychotic episode, we may have seen higher levels of executive dysfunction compared to the existing cohort. Thus, in this report, we are examining a 'best case scenario' cohort with respect to executive function, given that the population score is not as high as one would expect for SZ patients.[1] On the other hand, the data we obtained can be assumed to reflect the more typical performance of schizophrenia patients, most of whom are clinically stable most of the time.

FrSBE Score for Executive Dysfunction (Clinical Range: 65<130, Borderline: 60-64)		
	Before Illness	Present Time
SZ Group (*n* = 18)	72.39 +/- 20.89	64.11 +/-20.89
SA Group (*n* = 5)	54.25 +/- 22.70	59.5 +/- 17.14
All Patients (*n* = 23)	69.09 +/- 21.86	63.27 +/- 14.20

Table 2: FrSBE Test Scores for Executive Dysfunction
A list of the average scores for executive dysfunction using the FrSBE Self Rating Form is listed. Patients were asked to rate each statement presented in the FrSBE form from a scale of 1-5 on how the given phrase, such as "I feel confused" applies to oneself, with 1="Almost Never" and 5="Almost Always". Patients were asked to score themselves "Before Illness" and "At the Present Time". A score of 65-130 is determined to be in the clinical range. Scores between 60-64 are considered borderline.

3.2 SZ patients are bradykinetic and have higher noise in their moment-to-moment stochastic feedback than controls

We first present our results for the analysis of velocity-dependent kinematic parameters in our pointing task. Here we estimated the shape and the scale parameters of the continuous Gamma family of probability distributions with 95% confidence and plotted the results on the Gamma parameter plane. In this plane, along the shape (horizontal) *a*-axis the shape increases values towards the symmetric (Gaussian) PDF and decreases values towards the exponential PDF, special case when *a=1.* Along the scale (vertical) b-axis the estimated values increase the noise-to-signal ratio (the Fano Factor) whereas decreasing values indicate lower noise to signal ratio. **Fig. 5** depicts the empirically estimated Gamma parameters for the normalized peak angular velocity distributions for controls (red for goal-directed reach and blue for the supplementary retraction in **Fig. 5A**) and patients (green for goal-directed reach and black for supplementary retraction in **Fig. 5B**). It can be seen that the shape and scale parameters for the normalized peak angular velocity estimated PDF in the forward reach and uninstructed retraction in the control group cluster together more tightly in the low noise and high shape values (**Fig. 5A**). This indicates estimated

[1] While it has been estimated that over 90% of schizophrenia patients are characterized by impaired executive functioning[58], this is typically operationalized via neuropsychological test performance, and not by characterization of behavior, as was done in this study via the FRSBE. Therefore, the generalizability of our data to schizophrenia patients over the full range of neuropsychological functioning is not known. On the other hand, because the overwhelming majority of people with schizophrenia who are in treatment attend outpatient and partial hospital programs, we believe our data are generalizable to the non-acutely ill schizophrenia population. Also, because impairment in behavior (i.e., *disability*) is not always related to abnormal neuropsychological test performance (i.e., impairment)[59], including in schizophrenia[60], our results can be considered to generalize to a sample of schizophrenia patients with and without disability, even if their level of impairment is not well characterized.

PDFs with symmetric Gaussian shape and low dispersion. In the case of the patients, the estimated values exhibit a larger spread and many tend towards higher noise and lower shape values (**Fig. 5B**). Notice the noise exponential decay relation of the estimated Gamma parameters expressed as $f(x) = n \cdot x^{-m}$. The log-log relation revealed a linear fit shown in the insets, whereby the scatter aligns along the line of unity. The estimated coefficients for the power relation and the goodness of fit parameters are reported in the caption.

This log-relation with negative slope characterizing the noise in the speed-dependent parameter indicates that as the log of the estimated shape grows in value towards the symmetric Gaussian shape, the log of the noise to signal ratio linearly decays. **Table 3** lists the coefficients of each line equation and the goodness-of-fit characteristics, $\boldsymbol{p1}$ and $\boldsymbol{p2}$, in which $\boldsymbol{f(x) = p1 * x + p2}$. All fitted first-degree polynomial functions have an adjusted $\boldsymbol{R^2}$ value of close to 1, i.e., 0.9958 and 0.9955 for goal-directed movements and supplementary motions in controls, respectively (conditions are also abbreviated as CTRL FWD and CTRL BWD, correspondingly), and 0.9971 and 0.998 for goal-directed and supplementary motions in patients (SZ FWD and SZ BWD, respectively).

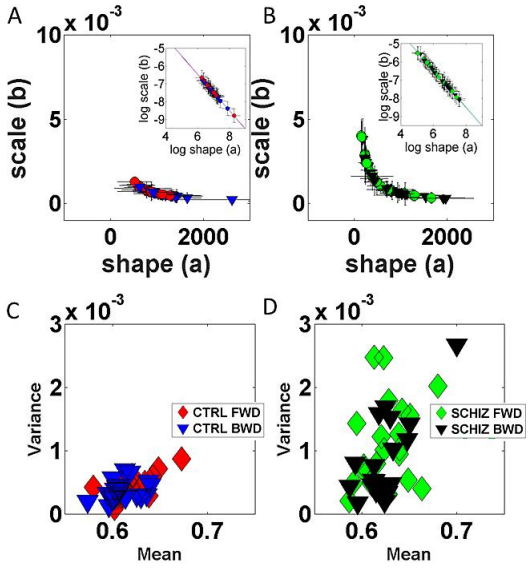

Fig. 5: Normalized peak velocity indices for neurotypical controls and SZ patients performing the pointing task

(A) Empirically estimated Gamma parameters plotted on the Gamma plane with 95% confidence intervals for normal controls; red for goal-directed reach and blue for the supplementary retraction**. (B)** Gamma stochastic signatures for the patients with SZ; green for goal-directed reach and black for supplementary retraction. In both cases a power law was found $f(x) = n \cdot x^{-m}$ with $n = 10^{-5}, m = 1.005,$ adjusted $R^2 \approx 0.99$ and RMSE on the order of 10^{-5} across conditions). Insets show the power relation fit to the log-log plots). Notice the SZ group exhibits higher levels of noise-to-signal (scale) values and concentrate towards the left (*a=1*) with lower shape values closer to the memory-less exponential distribution. **(C-D)** Gamma statistics plane estimated from the shape and scale parameters for controls **(C)** and SZ patients **(D)**. Notice the higher variability in the forward (deliberate) segments of the patients.

==========

First-Degree Least Squares Polynomial Equation: $f(x) = p1 * x + p2$				
	Neurotypical Controls		Schizophrenia Patients	
	Goal-Directed	**Supplementary**	**Goal-Directed**	**Supplementary**
p1 (95% CI)	-1.033 (-1.062, -1.004)	-1.02 (-1.05, -0.9908)	-1.011 (-1.035, -0.9871)	-1.025 (-1.046, -1.005)
p2 (95% CI)	-0.2538 (-0.4542, -0.05333)	-0.353 (-0.5602, -0.1458)	-0.402 (-0.55, -0.2541)	-0.3099 (-0.4408, -0.179)
SSE	0.01624	0.01343	0.02873	0.02066
R^2	0.996	0.9957	0.9973	0.9981
Adj. R^2	0.9958	0.9955	0.9971	0.998
RMSE	0.02717	0.0247	0.03699	0.03137

Table 3: Coefficients of the First-Degree Least-Squares Polynomial Function and Goodness-of-Fit Statistics corresponding to Normalized Peak Angular Velocity Gamma Parameters.

==========

The estimated first and second moments of the distributions for each individual were estimated as well. Thus, for the Gamma parameters $\mu = a \cdot b$ and $\sigma^2 = a \cdot b^2$ are plotted in **Figure 5** for controls (C) and patients (D) using the same color code as in A, B (see legend) for the forward and backward movement segments. This figure highlights the higher speed variance of the patients as expected from the higher noise to signal ratio.

Fig. 5C-D shows the individually estimated Gamma statistics (mean and variance) on the Gamma statistics plane. Note how levels of variance in the SZ group are quite high, notably in the goal-directed segment of the motor action (marked by green diamonds in **Fig. 5D**). We found striking differences between the patient and control groups in our error analysis (**Fig. 6**). As seen on the Gamma plane in **Fig. 5A-B**, the Fano Factor displays a higher spread of values in patients with SZ in both movement classes in relation to controls. Their trial-by-trial fluctuations in angular speed maxima have higher noise-to-signal ratio than controls. Specifically, in the forward segment of the motor trajectory, the higher Fano Factor is explained by the fact that patients with SZ exhibit statistically higher levels of variance in the rates of angular rotations of the hand as they reach towards the target with slower motions on average (**Fig. 5D**). Slower motions on average are evidenced in higher Gamma estimated mean of the normalized peak angular velocity index (nPV-index). Higher values of the nPV-index indicate that their average speed along each min-to-min segment (used in the denominator of this index and obtained as in **Figure 2C**) is lower than controls, thus leading the numerator of the nPV-index to have a higher value. The decrease in the mean paired with the increase in the variance contribute to the higher Fano Factor in the patients.

The results suggest that the SZ patients are bradykinetic and have higher noise in their moment-to-moment stochastic feedback. The sensory-motor signature in SZ is primarily characterized by high levels of uncertainty of both goal-directed and spontaneous segments' micro-movements. Note, however, that there is a reduction in the overall motor noise in the SZ scatter

dispersion corresponding to the spontaneous hand retraction (denoted as SCHIZ BWD and black triangles in **Fig. 5D**) in contrast to the controls with highly variable retractions. We consider this point later when we examine the corresponding trajectory symmetry-ratios.

3.3 Deliberate and spontaneous movement segments are indistinguishable in patients with SZ

We calculated the delta-error values according to each condition and mapped them to the Fano Factor calculations (**Fig. 6**). Recall that the scale parameter $\boldsymbol{b}$ is also the Fano Factor, as $\boldsymbol{FF} = \frac{\sigma_W^2}{\mu_W}$ (where $\boldsymbol{\sigma_W^2} = \boldsymbol{a}.\boldsymbol{b^2}$ and $\boldsymbol{\mu_W} = \boldsymbol{a}.\boldsymbol{b}$) reduces to $\boldsymbol{FF} = \boldsymbol{b}$. The scatter-box plot of the Fano Factor as a function of delta reveals that lower noise-to-signal ratio corresponds to lower delta values, indicating a tighter fit to the power law (**Fig. 6A, C**). In marked contast, as the Fano Factor increases in value (higher noise), delta increases as well, indicating departure from the power law. The latter characterizes the patients while the former characterizes the controls.

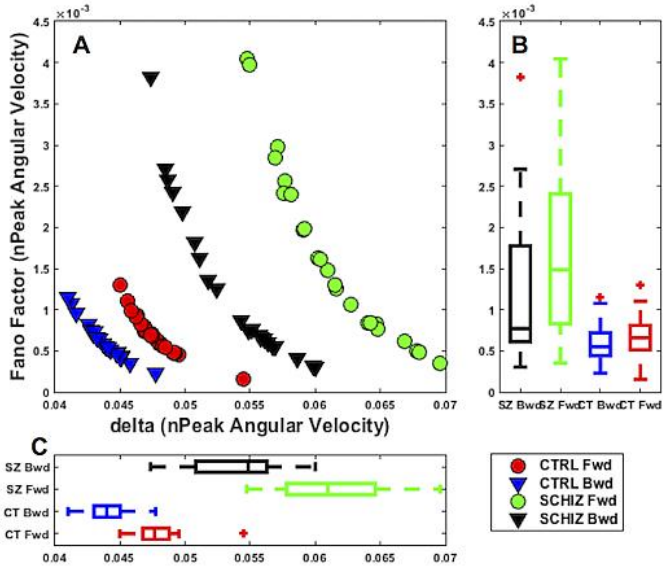

Fig. 6: Higher noise and departure from the power law in SZ: Mapping of Fano Factor *vs.* delta values for the normalized peak angular velocity distributions of the hand motions.
(A) Scatter and box plots of the Fano Factor (y-axis) as a function of delta values (x-axis) for the forward, goal-directed movement in controls (red circles) and the supplementary retraction (blue triangles). Goal directed and supplementary movements in the patient group are shown for comparison (green circles and black triangles, respectively). **(B-C)** Box plots against each respective axis designate median values. The edges of each boxplot represent the 25th and 75th percentiles of each subject group. Thick dotted lines on each end of the boxplot indicate values that are not considered outliers, and red plus signs indicate any outlier values. The range of values for both the Fano Factor and delta are much higher in the SZ group than in controls for both movement classes.

==========

The rates of change of these parameters are also different between patients and controls. This can be seen in the different slopes and intercepts of the lines that emerge when we fit a polynomial to each spread. The coefficients and goodness-of-fit calculations for this signature of motor-output variability are found in **Table 3**. The deliberate forward motions in the controls have the lowest

noise. This is in stark contrast to the forward motions of the patients with the highest noise-to-signal ratios.

Assessment of the significance of such statistical differences were done using the Wilcoxon Rank Sum Test. This yields the *p*-values associated with each condition comparison in **Table 4**. Note that the Fano Factors for the normalized peak angular velocity distributions are statistically different from one another when comparing the forward reaches in controls and patients, as well as in the retractions between our two subject pools. This finding translates to the delta comparisons, as delta values for the goal-directed control condition differ from patients' goal-directed movements. This separation between subject groups also holds true in the retraction. Delta values are statistically different for every group and movement class comparison. This is not the case for the comparison of goal directed patient reaches (SZ FWD) and supplemental patient motions (SZ BWD). This implies that, in marked contrast to controls, movement classes for patients with SZ are indistinguishable from one another in this velocity-dependent component. Whether the motion is deliberate or spontaneous cannot be discerned from the patients' micro-movements, in marked contrast to the controls' signatures of micro-movements.

Wilcoxon Rank Sum Test P-Values for Angular Velocity			
		Fano Factor	**Delta**
CTRL FWD	**CTRL BWD**	0.1245	0.0081*
CTRL FWD	**SCHIZ FWD**	1.4544e-04*	0.0013*
	SCHIZ BWD	0.0541	8.6219e-05*
CTRL BWD	**SCHIZ FWD**	1.9819e-05*	3.6796e-06*
	SCHIZ BWD	0.0051*	1.0391e-06*
SCHIZ FWD	**SCHIZ BWD**	0.1137	0.2720

Table 4: Wilcoxon Rank Sum Test for Velocity-Dependent Kinematic Parameters.
P-values are listed for the Wilcoxon Rank Sum Test for velocity-dependent kinematic parameters (Fano Factor and delta). An asterisk * indicates that $p < 0.05$, resulting in a significant difference between groups. The comparisons of the stochastic signatures of the normalized peak angular velocity index are pairwise between each row-element of column 1 and each row-element of column 2. For example CTRL FWD of row 2 column 1 is compared to SCHIZ FWD of row 2 column 2 (Fano Factor p-value of 1.4544e-04) and also with SCHIZ BWD of row 3 column 2 (Fano Factor p-value of 0.0541). The Fano Factor speaks of the dispersion of the estimated angular velocity-dependent PDF, while the Delta value speaks of the failure of the person's velocity-dependent stochastic signatures to follow a power law describing the noise decay, i.e. the noise decays exponentially as the distribution is more symmetric. This is captured in the linear relation of the log-log Gamma parameter plane. This relation that typically manifests in the controls tends to be statistically significantly different when comparing forward and backwards reaches between controls and SZ patients. The results denote problems in SZ with speed-dependent motor control and prediction of future trials based on current ones.

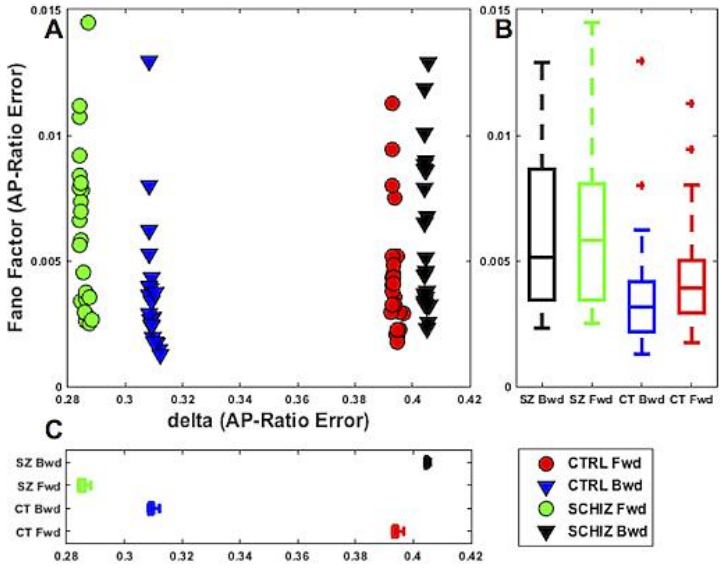

Fig. 7: Complementary roles of deliberate and spontaneous movements in SZ: Mapping of Fano Factor *vs.* delta values for hand trajectory geometric indexes.
(A) Scatter and box plots of the Fano Factor and delta values for the areas of the triangles that make up the error surface. Box plots against each axis designate median values. The horizontal edges of each boxplot represent the 25th and 75th percentiles of each subject group. Thick dotted lines on each end of the boxplot indicate values that are not considered outliers, and red plus signs indicate any outlier values. **(B)** Box plots of the Fano Factor (note the lower noise to signal ratios in controls). **(C)** Box plots of the delta values indicating the failure to follow the power law relation for each movement type (instructed forward *vs*. uninstructed backwards).

==========

3.4 Opposite patterns of volition in spontaneous retractions in SZ patients and controls

The area-perimeter ratio error triangulation revealed salient differences in spatial sensory-motor transformations (**Fig. 7**). We discovered that goal-directed movements in the patient population (green circles) have similar stochastic signatures as spontaneous retractions in the control group (blue triangles) (**Fig. 7A**). In marked contrast, the spontaneous retractions of the arm in patients (black triangles) produce patterns closely related to those found in the deliberate goal-directed movements in controls (red circles). This suggests that the spatial kinematics of goal directed motions in SZ patients are not under proper volitional control. Rather, the spontaneous segments, which are commonly so automated that they occur largely beneath awareness, are the ones that these patients seem to control better. This is relative to the normative stochastic signatures for deliberate motions (**Fig. 7C**). The variability in Fano Factor values in these geometric ratios is lower in controls for both movement classes than they are in the patient population (**Fig. 7B**). This result is consistent with the findings on velocity-dependent parameters, in which a wider distribution of normalized peak angular velocity measurements was also registered in SZ.

The Wilcoxon Rank Sum Test on the delta *vs.* Fano Factor values for the geometric trajectory ratios revealed that the Fano Factors of the area-perimeter ratio error triangulation surface are similar in all cases except within patient movement classes and between control and patient

supplementary movements (**Table 5**). As seen in **Fig. 7**, the automatic retractions of SZ patients are surprisingly close to the goal-directed actions in controls.

Wilcoxon Rank Sum Test P-Values Geometric Trajectory Ratios			
		Fano Factor (p-values)	**Delta (p-values)**
CTRL FWD	**CTRL BWD**	0.1768	3.0637e-09*
CTRL FWD	**SCHIZ FWD**	0.8565	0.0030*
	SCHIZ BWD	0.0788	9.7316e-09*
CTRL BWD	**SCHIZ FWD**	0.1979	4.5450e-09*
	SCHIZ BWD	5.4374e-04*	4.5450e-09*
SCHIZ FWD	**SCHIZ BWD**	3.0637e-09*	1.8357e-05*

Table 5: Wilcoxon Rank Sum Test for Geometric Trajectory Ratio Kinematic Parameters. P-values for the Wilcoxon Rank Sum Test are listed for the geometric trajectory ratios parameters (Fano Factor and delta). An asterisk * indicates that $p < 0.05$, indicating a significant difference between groups. The comparisons of the symmetry-related ratios from the hand trajectories are pairwise between each row-element of column 1 and each row-element of column 2. For example CTRL FWD of row 2 column 1 is compared to SCHIZ FWD of row 2 column 2 (Fano Factor p-value of 0.8565) and also with SCHIZ BWD of row 3 column 2 (Fano Factor p-value of 0.0788). The Fano Factor speaks of the dispersion of the estimated PDF for the hand trajectory geometric ratios, while the Delta value speaks of the failure of the person's trajectory-symmetry-dependent stochastic signatures to follow a power law describing the noise decay. The noise in the SZ patients significantly differs from controls in the backwards motions and from their own forward motions. The differences between SZ patients and controls regarding the predictive value of this symmetry trajectory parameter are significant for all comparisons, denoting lack of predictive value in SZ when examining the noise decay of impending trajectory ratios with respect to a given current trial. We refer the reader to the table in the Appendix summarizing the main results and possible interpretations in light of various aspects of motor control. These include volition, prediction, agency and action ownership.

4 Discussion

The present work characterized the stochastic signatures of fluctuations in motor performance (coined here micro-movements) inherently present in pointing motions of the hand en-route to visual targets. We obtained the ranges of the empirically estimated parameters of the continuous Gamma family of probability distributions for typical controls using the angular velocity as an internal parameter of interest and also utilizing external parameters such as those reflected by the geometrical aspects of the hand's motion trajectories. We then quantified these ranges for clinically stable patients with SZ and compared them to the normative data. The statistical signatures were estimated for parameters of the hand's continuous forward-and-back motions with an eye for possible differences between deliberate, goal-directed segments and spontaneous (uninstructed) segments as well. We found striking statistical differences between SZ patients and controls in all aspects of spatio-temporal kinematics and coordinate transformations that we investigated.

Patients with SZ showed higher noise and randomness in their velocity-dependent patterns relative to controls. Yet the surprising outcome was that the signatures of their spontaneous retracting motions, which are typically automatized and are thought to occur largely beneath awareness, were within the normal range of deliberateness in SZ patients. By marked contrast,

their goal-directed motions had the normative stochastic signatures found for spontaneous motions, i.e. they had higher uncertainty. It is possible that, in these patients, the afferent sensory information required to update internal forward models for anticipatory behavior is disrupted. A possible interpretation of these results is that the persistent excess noise quantified here in their continuously unfolding reaches may impede forward planning in SZ. Among brain areas thought to be important for forward computations within the framework of internal models for action are the cerebellum (*8, 60*) and the posterior parietal cortex (PPC) (*61*). The cerebellum is known to be a problematic brain area in SZ (*62-64*). Likewise, connectivity issues in SZ patients have been reported between parietal and motor cortices (*65, 66*). In light of the problems with the velocity-dependent signals that we have quantified here at the motor output level, it is possible that communication between these key nodes of the brain may be disrupted and the disruption may partly involve problems with continuous afferent and re-afferent inputs from the periphery.

Velocity-dependent peripheral input signals from self-produced goal-directed motions are an important source of guidance to the brain, to help compensate for synaptic transductions and transmission delays. In the context of visually guided reaches, areas in the posterior parietal cortex (PPC) are known to be important for the planning and execution of such actions. Regions in the PPC receive eye position and velocity afferent inputs via ascending prepositо-thalamo-cortical pathways (*67*). Proprioceptive inputs required for proper visuomotor geometric transformations for reaches (*55*) have been found as well to converge to the PPC (*68*) from the dorsal column nuclei and the postcentral somatosensory cortex. Given the putative roles of the PPC in forward prediction (*61*), trajectory formation (*69-71*), and geometric visuomotor transformations (*72, 73*) along with its cerebellar inputs to the lateral and medial intraparietal (LIP, MIP) cortical areas (*74*), we propose that the motor-PPC-cerebellar networks may be disrupted in SZ, and that part of this disruption is due to poor continuous updating involving afferent sensory guidance from more than one channel.

Afferent sensory channels convey reafferent kinesthetic signals from mechanoreceptors involving touch, pressure and ongoing self-produced movements. They also convey pain signals from nociceptors and temperature-related signals from thermoreceptors (*16*). The present work identifies deficits with kinesthetic reafference from ongoing movements, but it will be important to examine afferent deficits in SZ concerning thermo-regulation and pain perception, as these contribute to corporeal self-awareness. Corporeal self-awareness is critical in forward computations and geometric transformations, and both were found to be disrupted in SZ patients in the present results. Some work along those lines in SZ points to problematic areas in thermoregulation (*75-77*) and higher thresholds for pain perception relative to controls (*78-81*). The present results demonstrate that proper statistical analytics applied to continuous recordings are required to provide more meaningful answers to these questions and establish the nature of the relationships between these afferent inputs and specific sensory-motor deficits in anticipatory behavior and volitional control.

The signatures of micro-movements unveiled here in controls provide statistical information about the typical discrimination between different levels of intentionality and volition in controls. Specifically, the fluctuations in the movements of the controls can differentiate the segments that were instructed (goal-directed) from those which were not (spontaneous retractions). Here we see that such normative statistical information is absent from the movements of the patients with SZ. The deliberate and spontaneous segments of these patients contain moment-by-moment fluctuations in motor performace that have statistically indistinguishable signatures, as captured by their angular speed. Consistent with the lack of volitional control in the deliberate motions of SZ patients, the coordinate-transformation trajectory metric shows an inversion of the control schema in these patients whereby motions that are otherwise spontaneously occurring in controls are here

showing normative signatures of deliberateness. Interestingly, the pattern of reduced automaticity and a greater reliance on controlled processing has also been observed in visual perception in schizophrenia (reviewed in (*82, 83*)). This suggests that schizophrenia may be characterized by a generalized reduction in the ability to flexibly organize and automatize over-learned activity (*84*). However, we suggest that the quantitative methods we demonstrated, as applied to motor activity, provide an especially sensitive index of this dysfunction.

This work also adds a possible characterization of avolition whereby the sense of agency or ownership of motor control may be impeded in a system that cannot distinguish intended *vs.* spontaneous motions in typical ways. A possible interpretation is that the inversion of control signatures observed in these patients paired with the higher feedback uncertainty that noisy and random fluctuations in motor performance would bring back to the controllers in the brain may contribute to the lack of motor control agency. This in turn would exarcerbate symptoms of avolition and at a higher cognitive level contribute to a lack of a sense of action ownership. As such, lack of body or action ownership, measurable through fluctuations in motor performance of self-generated movements by the person (but unknown to the person) could be thouhgt of as basic foundational units of mental delusions or psychosis. In this sense it would be possible to derive objective indexes of fluctuations in motor performance, such as those explained here, to objectively characterize such observational symptoms using signals from the physical body.

Our data demonstrate the utility of quantifying the continuous flow of micro-movement output variability to help characterize disruptions of the sensory-motor system present in individuals with SZ. Our investigation into the sensory-motor patterns of patients with SZ indicates a high level of micro-motor noise and randomness in velocity-dependent signals, particularly in the goal-directed segment of the motor action loop (**Fig. 5D, Fig. 6**). We identify a source of random variability in the rates of angular rotations of the hand as it reaches towards the target and returns back to rest. It will be important to further investigate variability issues in the broader context of the DoF problem posed by Bernstein (*56*). This problem addresses possible brain-control strategies necessary for recruiting, releasing and coordinating the abundant number of DoF in the body so as to systematically accomplish a given set of goals. This next step in our investigation will be particularly important in light of other reports involving SZ patients with elevated levels of variability in motor-related tasks engaging the full body (*3, 85-87*). To the best of our knowledge, for the first time, we estimate the probability distributions governing these parameters in controls and SZ patients, specify their signatures, obtain their ranges for each group, and focus on disruptions in the rates of change in angular rotations of the hand. The empirically estimated Gamma statistics for normalized peak angular velocities in the patient group reveal bradykinetic motions with higher noise-to-signal ratios than normative ranges. We also wish to note that the analytic methods used here could be valuable for further refinement of the construct of dialipsis (i.e., sudden and random micro-episodes of degraded performance) as it has been associated with cognitive functioning in schizophrenia, e.g. (*88*) and schizotypy (*89*). Due to their novelty, it will be necessary to further validate these new methods across the broader spectrum of schizophrenia, including patients with more acute condition. Because of their sensitivity to subtle changes in motor output fluctuations at an individual level, it will be possible to test as well the effects of medication type and dosage across the spectrum of severity of this disorder.

In addition to our findings on velocity-dependent kinematic parameters, we discovered that geometric visuomotor transformations necessary to map internal joint rotations to hand target configurations (as well as to embody external targets in order to efficiently lead the hand to the goal) exhibit signatures similar to neurotypical controls in the spontaneous retractions (**Fig. 7**). This result could possibly serve as an objective marker of the level of disorganization for an

individual patient. The typical balance between intent and volition seems reversed for these movement classes in SZ patients. Our discovery that goal-directed movements are subject to more noise and randomness in SZ patients may contribute to our understanding of negative symptoms such as avolition (*35, 38, 90*). Because uninstructed supplementary motions in SZ were found to be slower and to exhibit normative signatures characteristic of deliberateness, they seem to require more conscious and effortful processing than is normal. This has implications for understanding the construct of hyper-reflexivity as applied to schizophrenia (*91, 92*): while this has been used to describe phenomenological disturbances in which tacit aspects of mental life are available to consciousness, the biological basis of this change has been explored only to a minimal extent.

5 Conclusions

In closing, the stochastic signatures of micro-movement variability that we describe adds great value to our current understanding of SZ by highlighting the significant contributions of the peripheral nervous system to our mental states and vice versa. Our findings point to disruptions in SZ not only in the brain, but also in the peripheral nervous system. We propose that perceptual abnormalities arise from a failure to properly embody the external environmental goals and integrate internal and external sensory inputs to convert such goals into meaningful self-produced actions with a proper sense of agency and ownership. Indeed, the integration of multiple sensory modalities may be compromised in SZ, leading to cognitive dysfunctions characteristic of the disorder and to the failure in visuomotor coordinate transformations that we uncovered in the breakdown of the trajectory symmetries. We introduced new indices based on the balance between movement classes with different levels of intent within the SZ population to show the value in objectively assessing (non-invasively) both goal-directed and goal-less movements with a higher level of individualized statistical precision than is commonly done. What had been traditionally treated as motor noise and thrown away or smoothed out as a nuisance in data turns out to be a very rich signal in our approach. We have offered a new unifying statistical framework to drive precision psychiatry initiatives forward, identifying peripheral nervous system changes that may correlate to the underlying pathophysiology of SZ.

6 Acknowledgements

This work was supported by the Nancy Lurie Marks Family Foundation Career Development Award to E.B. Torres, the NSF GRFP Award #DGE-0937373 to J. Nguyen, and the NIH Ruth L. Kirschstein NRS Award #T32-GM8339 from the NIGMS to J. Nguyen. Special thanks to the members of the Sensory-Motor Integration Lab, the Laboratory of Vision Research, and the Division of Schizophrenia Research at Rutgers for helping with recruitment and data collection.

7 References

1. R. S. Kahn, R. S. Keefe, Schizophrenia is a cognitive illness: time for a change in focus. *JAMA Psychiatry* **70**, 1107-1112 (2013).
2. P. D. Harvey, What is the evidence for changes in cognition and functioning over the lifespan in patients with schizophrenia? *J Clin Psychiatry* **75 Suppl 2**, 34-38 (2014).
3. J. S. Kent *et al.*, Motor deficits in schizophrenia quantified by nonlinear analysis of postural sway. *PLoS One* **7**, e41808 (2012).
4. V. Lerner, C. Miodownik, Motor symptoms of schizophrenia: is tardive dyskinesia a symptom or side effect? A modern treatment. *Curr Psychiatry Rep* **13**, 295-304 (2011).

5. M. Morrens, L. Docx, S. Walther, Beyond boundaries: in search of an integrative view on motor symptoms in schizophrenia. *Front Psychiatry* **5**, 145 (2014).
6. C. C. Pack, Eye movements as a probe of corollary discharge function in schizophrenia. *ACS Chem Neurosci* **5**, 326-328 (2014).
7. D. L. Levy, A. B. Sereno, D. C. Gooding, G. A. O'Driscoll, Eye tracking dysfunction in schizophrenia: characterization and pathophysiology. *Curr Top Behav Neurosci* **4**, 311-347 (2010).
8. M. Kawato, D. Wolpert, Internal models for motor control. *Novartis Found Symp* **218**, 291-304; discussion 304-297 (1998).
9. L. Lonini, L. Dipietro, L. Zollo, E. Guglielmelli, H. I. Krebs, An internal model for acquisition and retention of motor learning during arm reaching. *Neural Comput* **21**, 2009-2027 (2009).
10. E. Oztop, D. Wolpert, M. Kawato, Mental state inference using visual control parameters. *Brain Res Cogn Brain Res* **22**, 129-151 (2005).
11. E. B. Torres *et al.*, Autism: the micro-movement perspective. *Front Integr Neurosci* **7**, 32 (2013).
12. E. Von Holst, Relations between the central nervous system and the peripheral organs. *The British Journal of Animal Behaviour* **2**, 89-94 (1954).
13. E. Von Holst, H. Mittelstaedt, in *Perceptual Processing: Stimulus equivalence and pattern recognition*, P. C. Dodwell, Ed. (Appleton-Century-Crofts, New York, 1950), pp. 41-72.
14. A. Reichenbach, J. Diedrichsen, Processing reafferent and exafferent visual information for action and perception. *J Vis* **15**, 11 (2015).
15. T. A. Kuiken *et al.*, Targeted muscle reinnervation for real-time myoelectric control of multifunction artificial arms. *JAMA* **301**, 619-628 (2009).
16. D. Purves, *Neuroscience*. (Sinauer Associates, Sunderland, Mass., ed. 5th, 2012).
17. A. A. Faisal, L. P. Selen, D. M. Wolpert, Noise in the nervous system. *Nat Rev Neurosci* **9**, 292-303 (2008).
18. S. G. Sadeghi, M. J. Chacron, M. C. Taylor, K. E. Cullen, Neural variability, detection thresholds, and information transmission in the vestibular system. *J Neurosci* **27**, 771-781 (2007).
19. R. B. Stein, E. R. Gossen, K. E. Jones, Neuronal variability: noise or part of the signal? *Nat Rev Neurosci* **6**, 389-397 (2005).
20. H. P. Nguyen, J. B. Dingwell, Proximal versus distal control of two-joint planar reaching movements in the presence of neuromuscular noise. *J Biomech Eng* **134**, 061007 (2012).
21. E. B. Torres, The rates of change of the stochastic trajectories of acceleration variability are a good predictor of normal aging and of the stage of Parkinson's disease. *Frontiers in Integrative Neuroscience* **7:50**, (2013).
22. E. B. Torres, B. Lande, Objective and personalized longitudinal assessment of a pregnant patient with post severe brain trauma. *Front Hum Neurosci* **9**, 128 (2015).
23. E. B. Torres, J. Nguyen, C. Suresh, P. Yanovich, A. Kolevzon, in *The Society for Neuroscience*. (San Diego, CA, 2013).
24. G. Stanghellini *et al.*, The bodily self: a qualitative study of abnormal bodily phenomena in persons with schizophrenia. *Compr Psychiatry* **55**, 1703-1711 (2014).
25. K. Kahlbaum, *Catatonia*. (Johns Hopkins University Press, Baltimore,, 1973), pp. xviii, 102 p.

26. D. M. Rogers, *Motor disorder in psychiatry : towards a neurological psychiatry*. (J. Wiley & Sons, Chichester ; New York, 1992), pp. viii, 159 p.
27. E. Kraepelin, R. M. Barclay, G. M. Robertson, *Dementia præcox and paraphrenia*. (E. & S. Livingstone, Edinburgh,, 1919), pp. 1 p.
28. E. Bleuler, *Dementia praecox*. (International Universities Press, New York,, 1950), pp. 548 p.
29. D. Rogers, The motor disorders of severe psychiatric illness: a conflict of paradigms. *Br J Psychiatry* **147**, 221-232 (1985).
30. T. Insel *et al.*, Research domain criteria (RDoC): toward a new classification framework for research on mental disorders. *Am J Psychiatry* **167**, 748-751 (2010).
31. A. Caramazza, S. Anzellotti, L. Strnad, A. Lingnau, Embodied cognition and mirror neurons: a critical assessment. *Annu Rev Neurosci* **37**, 1-15 (2014).
32. A. Hasegawa *et al.*, Anterior cruciate ligament changes in the human knee joint in aging and osteoarthritis. *Arthritis Rheum* **64**, 696-704 (2012).
33. A. I. Goldman, *Simulating minds : the philosophy, psychology, and neuroscience of mindreading*. Philosophy of mind (Oxford University Press, Oxford ; New York, 2008), pp. 364 p.
34. I. Bombin, C. Arango, R. W. Buchanan, Significance and meaning of neurological signs in schizophrenia: two decades later. *Schizophr Bull* **31**, 962-977 (2005).
35. D. M. Barch, E. C. Dowd, Goal representations and motivational drive in schizophrenia: the role of prefrontal-striatal interactions. *Schizophr Bull* **36**, 919-934 (2010).
36. J. Bender *et al.*, Neural correlates of impaired volitional action control in schizophrenia patients. *Psychophysiology* **50**, 872-884 (2013).
37. B. Reuter, M. Jager, R. Bottlender, N. Kathmann, Impaired action control in schizophrenia: the role of volitional saccade initiation. *Neuropsychologia* **45**, 1840-1848 (2007).
38. F. Tremeau, K. A. Nolan, D. Malaspina, D. C. Javitt, Behavioral validation of avolition in schizophrenia. *Schizophr Res* **138**, 255-261 (2012).
39. E. B. Torres, Two classes of movements in motor control. *Exp Brain Res* **215**, 269-283 (2011).
40. E. B. Torres, A. Raymer, L. J. Gonzalez Rothi, K. M. Heilman, H. Poizner, Sensory-spatial transformations in the left posterior parietal cortex may contribute to reach timing. *J Neurophysiol* **104**, 2375-2388 (2010).
41. E. B. Torres, K. M. Heilman, H. Poizner, Impaired endogenously evoked automated reaching in Parkinson's disease. *J Neurosci* **31**, 17848-17863 (2011).
42. E. B. Torres, Signatures of movement variability anticipate hand speed according to levels of intent. *Behavioral and Brain Functions* **9**, 10 (2013).
43. S. Hawgood, I. G. Hook-Barnard, T. C. O'Brien, K. R. Yamamoto, Precision medicine: Beyond the inflection point. *Sci Transl Med* **7**, 300ps317 (2015).
44. T. R. Insel, The NIMH Research Domain Criteria (RDoC) Project: precision medicine for psychiatry. *Am J Psychiatry* **171**, 395-397 (2014).
45. J. A. Bernard, V. A. Mittal, Updating the research domain criteria: the utility of a motor dimension. *Psychol Med*, 1-5 (2015).
46. J. E. Mosimann, Size Allometry: Size and Shape Variables with Characterizations of the Lognormal and Generalized Gamma Distributions. *Journal of the American Statistical Association* **65**, 930-945 (1970).

47. H. Shimazaki, S. Shinomoto, A method for selecting the bin size of a time histogram. *Neural Comput* **19**, 1503-1527 (2007).
48. D. Freedman, P. Diaconis, On the histogram as a density estimator: L theory. *Probability Theory* **57**, 453-476 (1981).
49. S. M. Ross, *Introduction to probability and statistics for engineers and scientists*. (Elsevier, Amsterdam, ed. Fifth edition., 2014), pp. pages cm.
50. P. Yanovich, R. W. Isenhower, J. Sage, E. B. Torres, Spatial-orientation priming impedes rather than facilitates the spontaneous control of hand-retraction speeds in patients with Parkinson's disease. *PLoS ONE* **8**, 1-19 (2013).
51. J. Lleonart, J. Salat, G. J. Torres, Removing allometric effects of body size in morphological analysis. *J Theor Biol* **205**, 85-93 (2000).
52. U. Fano, Ionization Yield of Radiations. II. The Fluctuations of the Number of Ions. *Physical Review* **72**, 26 (1947).
53. E. B. Torres, Atypical signatures of motor variability found in an individual with ASD. *Neurocase: The neural basis of cognition* **1**, 1-16 (2012).
54. V. Kalampratsidou, E. Torres, Exploring new wearable sensing technology in perceptual experiments. *J Vis* **15**, 979 (2015).
55. E. B. Torres, D. Zipser, Reaching to grasp with a multi-jointed arm. I. Computational model. *J Neurophysiol* **88**, 2355-2367 (2002).
56. N. Bernstein, *The co-ordination and regulation of movements*. (Oxford Press, Oxford, 1967).
57. E. B. Torres, D. Zipser, Simultaneous control of hand displacements and rotations in orientation-matching experiments. *J Appl Physiol* **96**, 1978-1987 (2004).
58. E. B. Torres, New symmetry of intended curved reaches. *Behav Brain Funct* **6**, 21 (2010).
59. B. Delaunay, Sur la sphere vide. *Izv. Akad. Nauk SSSR, Otdelenie Matematicheskii i Estestvennyka Nauk* **7**, 1-2 (1934).
60. M. Kawato *et al.*, Internal forward models in the cerebellum: fMRI study on grip force and load force coupling. *Prog Brain Res* **142**, 171-188 (2003).
61. G. H. Mulliken, S. Musallam, R. A. Andersen, Forward estimation of movement state in posterior parietal cortex. *Proc Natl Acad Sci U S A* **105**, 8170-8177 (2008).
62. B. C. Ho, C. Mola, N. C. Andreasen, Cerebellar dysfunction in neuroleptic naive schizophrenia patients: clinical, cognitive, and neuroanatomic correlates of cerebellar neurologic signs. *Biol Psychiatry* **55**, 1146-1153 (2004).
63. H. Picard, I. Amado, S. Mouchet-Mages, J. P. Olie, M. O. Krebs, The role of the cerebellum in schizophrenia: an update of clinical, cognitive, and functional evidences. *Schizophr Bull* **34**, 155-172 (2008).
64. J. A. Bernard, V. A. Mittal, Cerebellar-motor dysfunction in schizophrenia and psychosis-risk: the importance of regional cerebellar analysis approaches. *Front Psychiatry* **5**, 160 (2014).
65. G. Koch *et al.*, Connectivity between posterior parietal cortex and ipsilateral motor cortex is altered in schizophrenia. *Biol Psychiatry* **64**, 815-819 (2008).
66. M. Yildiz, S. J. Borgwardt, G. E. Berger, Parietal lobes in schizophrenia: do they matter? *Schizophr Res Treatment* **2011**, 581686 (2011).

67. V. Prevosto, W. Graf, G. Ugolini, Posterior parietal cortex areas MIP and LIPv receive eye position and velocity inputs via ascending preposito-thalamo-cortical pathways. *Eur J Neurosci* **30**, 1151-1161 (2009).
68. V. Prevosto, W. Graf, G. Ugolini, Proprioceptive pathways to posterior parietal areas MIP and LIPv from the dorsal column nuclei and the postcentral somatosensory cortex. *Eur J Neurosci* **33**, 444-460 (2011).
69. M. Hauschild, G. H. Mulliken, I. Fineman, G. E. Loeb, R. A. Andersen, Cognitive signals for brain-machine interfaces in posterior parietal cortex include continuous 3D trajectory commands. *Proc Natl Acad Sci U S A* **109**, 17075-17080 (2012).
70. G. H. Mulliken, S. Musallam, R. A. Andersen, Decoding trajectories from posterior parietal cortex ensembles. *J Neurosci* **28**, 12913-12926 (2008).
71. E. B. Torres, R. Quian Quiroga, H. Cui, C. A. Buneo, Neural correlates of learning and trajectory planning in the posterior parietal cortex. *Front Integr Neurosci* **7**, 39 (2013).
72. C. A. Buneo, R. A. Andersen, The posterior parietal cortex: sensorimotor interface for the planning and online control of visually guided movements. *Neuropsychologia* **44**, 2594-2606 (2006).
73. C. A. Buneo, M. R. Jarvis, A. P. Batista, R. A. Andersen, Direct visuomotor transformations for reaching. *Nature* **416**, 632-636 (2002).
74. V. Prevosto, W. Graf, G. Ugolini, Cerebellar inputs to intraparietal cortex areas LIP and MIP: functional frameworks for adaptive control of eye movements, reaching, and arm/eye/head movement coordination. *Cereb Cortex* **20**, 214-228 (2010).
75. T. W. Chong, D. J. Castle, Layer upon layer: thermoregulation in schizophrenia. *Schizophr Res* **69**, 149-157 (2004).
76. R. Shiloh, A. Weizman, R. Stryjer, N. Kahan, D. A. Waitman, Altered thermoregulation in ambulatory schizophrenia patients: a naturalistic study. *World J Biol Psychiatry* **10**, 163-170 (2009).
77. H. Hermesh *et al.*, Heat intolerance in patients with chronic schizophrenia maintained with antipsychotic drugs. *Am J Psychiatry* **157**, 1327-1329 (2000).
78. A. Kudoh, H. Ishihara, A. Matsuki, Current perception thresholds and postoperative pain in schizophrenic patients. *Reg Anesth Pain Med* **25**, 475-479 (2000).
79. M. Urban-Kowalczyk, J. Pigonska, J. Smigielski, Pain perception in schizophrenia: influence of neuropeptides, cognitive disorders, and negative symptoms. *Neuropsychiatr Dis Treat* **11**, 2023-2031 (2015).
80. G. Engels *et al.*, Clinical pain in schizophrenia: a systematic review. *J Pain* **15**, 457-467 (2014).
81. M. Levesque *et al.*, Pain perception in schizophrenia: evidence of a specific pain response profile. *Pain Med* **13**, 1571-1579 (2012).
82. P. J. Uhlhaas, S. M. Silverstein, Perceptual organization in schizophrenia spectrum disorders: empirical research and theoretical implications. *Psychol Bull* **131**, 618-632 (2005).
83. S. M. Silverstein, B. P. Keane, Perceptual organization impairment in schizophrenia and associated brain mechanisms: review of research from 2005 to 2010. *Schizophr Bull* **37**, 690-699 (2011).
84. W. A. Phillips, S. M. Silverstein, Convergence of biological and psychological perspectives on cognitive coordination in schizophrenia. *Behav Brain Sci* **26**, 65-82; discussion 82-137 (2003).

85. E. S. Kappenman *et al.*, Electrophysiological Evidence for Impaired Control of Motor Output in Schizophrenia. *Cereb Cortex,* (2015).
86. E. Lallart *et al.*, Gait control and executive dysfunction in early schizophrenia. *J Neural Transm* **121**, 443-450 (2014).
87. M. Teremetz *et al.*, Deficient grip force control in schizophrenia: behavioral and modeling evidence for altered motor inhibition and motor noise. *PLoS One* **9**, e111853 (2014).
88. S. Matthysse, D. L. Levy, Y. Wu, D. B. Rubin, P. Holzman, Intermittent degradation in performance in schizophrenia. *Schizophr Res* **40**, 131-146 (1999).
89. M. W. Roche, S. M. Silverstein, M. F. Lenzenweger, Intermittent Degradation and Schizotypy. *Schizophr Res Cogn* **2**, 100-104 (2015).
90. G. Foussias, G. Remington, Negative symptoms in schizophrenia: avolition and Occam's razor. *Schizophr Bull* **36**, 359-369 (2010).
91. L. A. Sass, Self-disturbance and schizophrenia: structure, specificity, pathogenesis (Current issues, New directions). *Schizophr Res* **152**, 5-11 (2014).
92. L. A. Sass, J. Parnas, Schizophrenia, consciousness, and the self. *Schizophr Bull* **29**, 427-444 (2003).
93. E. Torres, R. Andersen, Space-time separation during obstacle-avoidance learning in monkeys. *J Neurophysiol* **96**, 2613-2632 (2006).
94. H. H. Yang, S. Amari, Complexity issues in natural gradient descent method for training multilayer perceptrons. *Neural Comput* **10**, 2137-2157 (1998).
95. A. Gray, *Modern differential geometry of curves and surfaces*. Studies in advanced mathematics (CRC Press, Boca Raton, 1993), pp. xviii, 664 p.
96. E. B. Torres, J. Cole, H. Poizner, Motor output variability, deafferentation, and putative deficits in kinesthetic reafference in Parkinson's disease. *Front Hum Neurosci* **8**, 823 (2014).
97. E. Torres, J. Cole, H. Poizner, in *The Society for Neuroscience Annual Meeting*. (New Orleans, LA, 2012).

8 Appendix

The symmetry used to characterize the trajectories of the hand to the target emerges from a theoretical formulation of a geometric solution to the redundancy-problem (*55, 58, 93*). The redundancy problem seeks to find a unique solution inverse map from a desirable hand configuration to a unique bodily posture that efficiently accomplishes a goal-directed action. It is a difficult problem because the forward map from postures to the desired hand position and orientation is many-to-one. The question is how the nervous system attains a consistent solution invariant to changes in the dynamics of the motions. In the proposed (geometric) solution a local linear isometric embedding is provided to locally solve the problem of finding a displacement of the hand (denoted (Δx)) in the external space that linearly corresponds to a displacement in the internal space of joint configurations (denoted (Δq).) Recursively, the proposed solution

$dq = G_q^{-1} \cdot \left(r \circ f\left(x^{\text{target}}, q^{\text{init}} \right) \right) \cdot \Delta\tau$ (the Torres-Zipser PDE (*55*)) builds a path connecting the initial arm-hand configuration to the target (the desirable hand configuration) and the solution path is also found in the internal configuration space Q of joint angles. The solution curve in the external X space follows a symmetry that is dynamic invariant.

The solutions previously proposed were non-unique because the internal Q-space has many more dimensions than the external X-space. Thus to each point in X there correspond infinite points in Q; i.e. to each hand location in peripersonal space there correspond many postural configurations of the arm. By choosing the 'natural gradient' (*55, 94*) of Q-space at the local point q (i.e. the small rotation of the joints (Δq) that moves the hand towards the target by a linearly related a small amount (Δx)) it is possible to uniquely construct a path in Q with a corresponding path in X whereby both are geodesics (i.e. find the shortest distance curve joining the initial hand position and the target) in each corresponding space. By 'natural gradient' here we mean that the appropriate distance metric (the norm) used to select the appropriate gradient direction shall be selected according to the coordinate functions defining the forward kinematics map, the task and context (e.g. numerically approximated (*93*)). The appropriate gradient is the true minimizing direction in Q-space that uniquely maps to the true minimizing direction in X-space, thus pulling the hand to the target location.

In the optimization framework that we used, the cost surface represents at each point in Q (i.e. at each posture) how far from the target the hand is according to the internal configuration space. Thus at a point in postural configuration space the hand is at some distance from the target. This distance does not need to be Euclidean as it depends on the task and context (see (*55, 93*) for examples of possible distances used to model different tasks and different contexts). The curvature of the cost surface will depend on the choice of distance and so will the choice of gradient to construct the motion curve in a geometrically optimal (geodesic) way. Notice here that under appropriate gradient (as selected by the appropriate distance norm $G_q^{\mu} = J^t G_x^{\alpha} J$ (*95*) where J is the Jacobian coordinate transformation matrix of the forward kinematics map from Q to X and G are the first fundamental forms or metric tensors of Q and X respectively) no local minima will plague this procedure when descending along the cost surface to the unique global minimum that is being searched, i.e. the posture at which the hand-target distance is minimal.)

When the proper distance relation is used to make this a distance-preserving inverse map and as such, to select the gradient direction in Q corresponding one-to-one to the desirable gradient direction in X, the gradient in Q is the principal eigenvector of the Hessian matrix (the second fundamental form) and the tangent vector to the geodesic curved being built is locally, at each point of this curve, parallel to the normal to the above mentioned cost surface at each point of the curve. Under these conditions the non-Euclidean geodesic curve being built to geometrically describe the motion path can be transformed into other geodesic curve (e.g. the Euclidean one) and the point where the planar curvature deviation of the non-Euclidean straight line to the Euclidean straight line is maximal leads to the symmetry uncovered by the area-perimeter relations between the two curves (*58*).

This is the theoretical scenario, but as it turns out, the empirical scenario where we test the predictions of these theoretical models yield similar relations in humans (*40, 41*) and non-human (*58*) primates performing reaching and reach-to-grasp movements, and doing so also around obstacles. In humans, we know that these symmetries are not merely the byproduct of biomechanical constraints but rather under brain cognitive control. This is so because they do break down in patients of various types but can be ***selectively*** improved in each population as a function of the form of sensory feedback employed to guide the reach. Thus in a parietal patient who suffered a localized stroke in the left hemisphere the symmetry broke down but was recovered towards normal levels when we provided the patient with continuous visual feedback of the target location (by continuously lighting the target in the dark as he pointed to it) (*40*). In patients with mild Parkinson's disease (PD) this type of feedback was not useful, as measured by the symmetry. This form of feedback made the spread error broader and the relation between the area and perimeter ratios non-linear. Instead, their system with PD benefited from placing the continuous feedback as a light on the moving finger (*41*). The alignment of vision and proprioception in these PD patients over compensated the noisy proprioception found as well in these patients (*96*) and recovered the area-perimeter symmetry. The symmetry in the theoretical model is exactly ½ but in the real empirical data there is sensory-motor noise and as such there is rather a scatter around the ½ values of the area ratio and the perimeter ratio. How the shape of this scatter changes in SZ is explored here using the methods described in the main text. We search for departures from the symmetry (½- values) and from departures of the scatter of points from the line of unity when the hand reaches forward and when it retracts. The normative data produces a scatter around ½ and has good linear fit around the scatter of points from trial to trial that produce slope close to 1. In

such cases the coordinate transformations from desirable hand to posture configuration are intact (*40*) and the balance between intended and spontaneous motions intact (*97*).

9 Summary Table

Metric/Technique	Differences between SZ and Typical Participants	Interpretation on the Relationships to Control, Volition, Agency and Action Ownership
Gamma parameter estimation from fluctuations in angular velocity during pointing	Different families of PDFs were found in patients and controls with statistically significant differences in the scale parameter denoting the Fano Factor (noise to signal ratio). Patients had significantly higher noise and a larger tendency to distributions away from the symmetric Gaussian as compared to controls	Higher noise and more random fluctuations ought to negatively impact the kinesthetic feedback from moment to moment, ultimately impeding predictive motor control. Typical ranges of these parameters were more Gaussian and with less dispersion than SZ. (Figure 5 AB and Table 4)
Mean and Variance estimation	Patients had on average more variable rates of angular rotation and were on average slower, giving rise to higher values of the index because of lower values of average speed in the denominator. The differences were statistically significant as well and primarily accounted for the higher levels of noise to signal ratio (higher values of the scale parameter) in SZ.	More variable angular speed is harder to control and predict from trial to trial and slower motions that are otherwise fast and automatic in controls are indicative of poor autonomy in the system. Excess supervision on motions that should be automated may lead to such slowness in rotational joint control and introduce undesirable variability in movements that would otherwise go unnoticed.
Linear Fit of the log-log scatter from the estimated shape-scale values based on the angular velocity values for each participant	Both patients and controls had a good linear fit to the scatter of the log-log estimated Gamma parameters but patient's Delta error was significantly higher than controls (Table 4) as was their Fano Factor.	The excess error in SZ denotes failure to accurately predict with high certainty future angular speed maxima based on current speed performance. Under more random PDFs towards the exponential range of the Gamma parameter plane the lack of predictive value may also impede establishing from moment to moment cause and effect relations between self-produced movements and ownership of those movements. If the person's motor system often fails to gain confirmation of

		predicting ahead the rate of change of its motions, then uncertainty about agency may increase (e.g. who is in control?; who has autonomy over these motions?) and eventually lead to a poor sense of action ownership
Symmetry measuring integrity of coordinate transformation	Patients with SZ manifested profound differences in the trajectory geometric ratio between forward (deliberate) and backwards (spontaneous) movements. These are characterized by a break in the symmetry and also in the slope of unity for both motions (Figure 3 shows this clearly). This indicates a lack of conservation in the transformation of coordinates mapping internal angular velocities of the joints to external velocities of the hand.	Under failure of proper coordinate transformations the solution of the redundant DoF problem is not appropriately implemented by the system with SZ. Thus it must be difficult to coordinate the DoF and generate appropriate synergies that help the sensory-motor system self-organize complex motions. The lack of proper coordination across bodily motor functions can lead to improper organizational mental skills via poor planning strategies and overall impede the volitional control of movements.
Linear Fit of the log-log scatter from the estimated shape-scale values based on fluctuations of the trajectory-symmetry ratios for each participant	An inversion of patterns emerged in the analyses of the Fano Factor and Delta error from the scatter derived from the geometric ratios and the Gamma parameter estimation when considering deliberate and spontaneous movements (Figure 7 and Table 5). The differences were statistically significant.	The SZ patients manifested normative signatures spontaneous movements in their deliberate forward pointing motions. Typically spontaneous motions go unnoticed by controls, reportedly occurring largely beneath awareness in various contexts (including boxing and perceptual tasks involving visual illusions). The automatic control of such transitional motions can be interpreted as a good sign of autonomy supplementing the deliberate performance of forward movements to a goal. Normally, consistency and good balance of this dichotomy of deliberateness and spontaneity is good to help anticipate the sensory-motor consequences of one's own actions and intentions. The absence and reversion of such patterns in SZ suggests a poor sense of action ownership in the precise sense that a movement that the person is supposed to control at will to achieve a precise goal is actually spontaneously happening. Under such conditions, how would that person deduce with some degree

		of statistical certainty that the spontaneous random movement is its own?